Towards an Ultra Wideband Low Noise Active Sinuous Feed for Next Generation Radio Telescopes

Rohit Gawande, *Student Member, IEEE*, and Richard Bradley, *Member, IEEE*

***Abstract*—Next generation of instruments for radio astronomy will benefit greatly from reflector antenna feeds that demonstrate very wide instantaneous bandwidth and exhibit low noise behavior. Our study focuses on design and measurement of an ultra-wideband inverted conical sinuous antenna and its integration with a low noise pseudo differential amplifier. The self-complementary, frequency independent nature of the planar sinuous geometry results in a nearly constant beam pattern and fixed phase center over more than a 10:1 operating frequency range. In order to eliminate the back-lobe response over such a wide frequency range, we have projected the sinuous pattern onto a cone, and a ground plane is placed directly behind the cone's apex. This inverted, conical geometry assures wide bandwidth operation by locating each sinuous resonator a quarter wavelength above the ground plane. The presence of a ground plane near a self complementary antenna destroys the self complementary nature of the composite structure resulting in frequency dependent impedance variations. We demonstrate, using simulations and measurements, how the return loss can be improved by modifying the sinuous geometry. A physically smaller, laboratory version of the 0.3 to 3 GHz antenna that is truncated to operate from 1 to 3 GHz was fabricated to verify proper LNA-feed integration through careful modeling and measurements. Over this range, a return loss of better than 9 dB is measured while simulations indicate a nearly constant beam pattern. A full decade bandwidth, low noise amplifier was specially designed for noise match to the higher terminal impedance encountered by this antenna yielding an improved sensitivity over what is possible with conventional 50 Ω amplifiers. A measured system noise temperature of less than 100 K is reported. Based on these results, we will increase the bandwidth of the system to 10:1 by simply attaching additional resonators to the sinuous arms.**

***Index Terms*—Decade bandwidth, low noise, sinuous, ultrawideband, Y-factor, $A/T_{\rm sys}$.**

I. Introduction

THERE is an increasing interest in wideband, low noise feeds for the next generation radio telescopes. Ultra wideband feeds are essential for sweeping over large frequency ranges, frequency agility, detection of short duration pulses, multi-frequency imaging, and simultaneous observation of several spectral lines.

Manuscript received April 15, 2010; revised January 03, 2011; accepted January 15, 2011. Date of publication March 03, 2011; date of current version June 02, 2011.

R. Gawande is with the Department of Electrical and Computer Engineering, University of Virginia, Charlottesville, VA 22903 USA (e-mail: rgawande@nrao.edu).

R. Bradley is with National Radio Astronomy Observatory, Charlottesville, VA 22903 USA (e-mail: rbradley@nrao.edu).

Color versions of one or more of the figures in this paper are available online at http://ieeexplore.ieee.org.

Digital Object Identifier 10.1109/TAP.2011.2122238

In the past, wide bandwidth feeds have been developed using log periodic structures of line resonators or elements stacked in the form of pyramid such as, e.g., zig-zag elements used in Allen Telescope Array [1] or the trapezoidal geometry used in Green Bank Solar Radio Burst Spectrometer (GB/SRBS) [2]. Such a feed, however, has a phase center that varies with frequency. The Eleven Antenna developed by the Chalmers group solves the varying phase center problem [3], [4]. The commercially available open boundary quadridge horn [5] and the quasi self-complementary (QSC) feed being developed at Cornell [6] are other examples of decade bandwidth feeds.

In the past, we have developed a wideband, fixed phase center, dual polarized, low loss feed with an integrated low noise amplifier (LNA). Initial results of this study can be found in [7] and [8]. The far field patterns of the feed-LNA integrated unit were measured including E, H, Co-, and Cross-polarization over the 0.5–4 GHz frequency range. The beamwidth was nearly constant and the phase center remained close to the center of the ground plane over the entire frequency range. However, we found that overall antenna lost the self-complementary nature in the presence of the ground plane which led to frequency dependent impedance variations. Similar observations can be found elsewhere in the literature [9], [10].

We are presenting the results of a parameter study to improve return loss with non-interleaving versions of the sinuous antenna in the presence of a ground plane. Based on the results of the parameter study we plan to build a decade bandwidth, ambient temperature feed integrated with an LNA. For the ease of integration and initial testing, the feed size is kept small which limits the low frequency operation to about 1 GHz. This truncated version (1 to 3 GHz) of the actual decade bandwidth (0.3 to 3 GHz) feed is characterized here. The LNA is designed for the 0.3 to 3 GHz range and hence the operation of this prototype unit could in principle be easily extended to lower frequencies by attaching additional resonators in each arm in near future.

The sensitivity of an antenna and its receiving system can be expressed as a $G/T_{\rm sys}$ ratio, where G is the gain of the parabolic dish illuminated by a feed and $T_{\rm sys}$ is the system noise temperature. A comparative study of different wideband topologies with $G/T_{\rm sys}$ as the figure of merit can be found in [11]. In radio astronomy, a frequency independent figure of merit $A/T_{\rm sys}$ is used instead of $G/T_{\rm sys}$, where, A is the effective area of the parabola. We are presenting a discussion in terms of $A/T_{\rm sys}$ for the current system in light of the improved input return loss and with a pseudo differential low noise amplifier.

The theory and working principle of the antenna is presented in Section II. The results of a parameter study to improve the input return loss is presented in Section III. In Section IV,

0018-926X/$26.00 © 2011 IEEE

we discuss the measured and simulated performance of the antenna. Low noise amplifier design and assembly is covered in Section V. Measurement of the receiver noise using the Y-factor method and overall $A/T_{\rm sys}$ performance is discussed in Sections VI and VII, respectively. The challenges and possible future direction for the development of a decade bandwidth feed suitable for radio astronomy is discussed in Section VIII.

II. Sinuous Antenna Theory

The planar sinuous antenna proposed by DuHamel [12] is a frequency independent structure with constant beamwidth, fixed phase center, constant input impedance, low loss and orthogonal senses of linear polarization. As shown in Fig. 1(a), a sinuous curve is defined as

$$\Phi = \alpha \sin\left(2\pi C \frac{\ln r - \ln r_{\min}}{\ln r - \ln r_{\max}}\right) \tag{1}$$

where Φ is the polar angle, r is the radius, α is the angle subtended by the arc, and C is the number of resonators. $r_{\min}$ and $r_{\max}$ are inner and outer radii [13] of the antenna, respectively. One sinuous arm is formed by rotating this curve by $\pm\delta$ around the origin as shown in Fig. 1(b). A four arm antenna structure is created by rotating a single arm through 90 degree increments to form a self-complementary antenna as shown in Fig. 1(c). The condition for a N-arm sinuous structure to be self complementary is $\delta = \pi/2N$. The curves in Fig. 1 are drawn using parameters $\alpha = \pi/4$ and $\delta = \pi/8$. The arm-to-virtual-ground terminal impedance for a self-complementary N-arm structure fed in mode m is frequency independent and given by [14]

$$Z_m = \frac{30}{\pi}\sin\left(\frac{\pi m}{N}\right) \tag{2}$$

where Z_m is equal to 133 Ω for a 4 arm structure excited in mode $m = 1$. Voltage excitation for a normal mode is given by [13]

$$V_{n,m} = A_m \exp(j360\, mn/N) \tag{3}$$

where n is the arm number, m is the mode number and A_m is the excitation amplitude of mode m.

Log periodic nature of the antenna is such that resonators follow a geometric progression. The ratio of radii for any two consecutive resonators is constant and defined as the expansion parameter τ. The active region of the sinuous antenna is defined where the resonator length is approximately equal to $\lambda/2$. In a four arm structure, the opposing arms are fed 180° out of phase. The charges in opposite pairs of arms flow in the same direction to form linearly polarized beams that are mutually orthogonal. The active region migrates inward from one resonator to another as the frequency of operation increases and provides a constant beamwidth. The lower frequency of operation is limited by the size of the antenna to

$$\lambda_L = 4r_{\max}(\alpha + \delta) \tag{4}$$

but in practice is slightly higher because of the edge effect. The abrupt termination of the antenna at the outer resonator causes a reflection from the edge, hence one or two additional resonators should be used to assure the optimum low frequency operation.

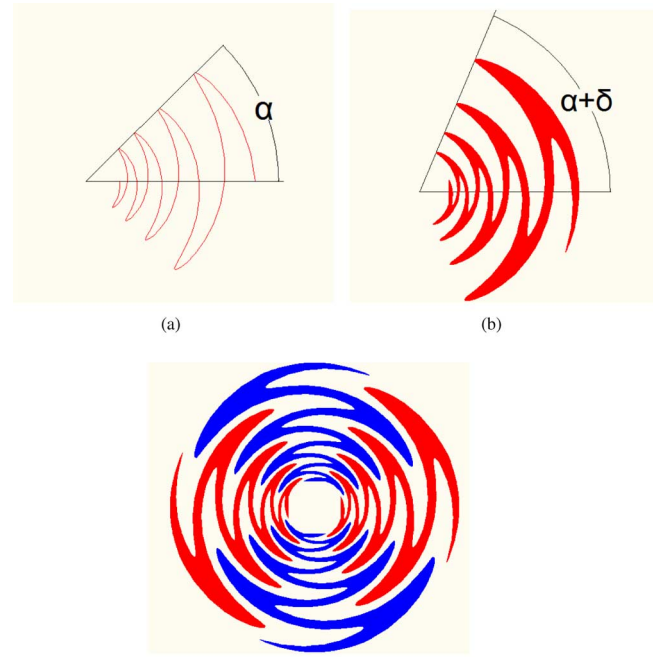

Fig. 1. Planar sinuous antenna. (a) Sinuous curve, (b) Sinuous arm, (c) Four arm structure.

The high frequency limit is set by the feed point structure. In order to provide a good transition from feed point to the active region, the smallest segment should be less than $\lambda_H/4$ where $\lambda_H = 8r_{\min}(\alpha + \delta)$ which defines the high frequency limit [13]. The phase center is fixed in position due to symmetry of the geometry.

The planar sinuous antenna radiates in both directions. This bidirectional nature can be converted to an unidirectional antenna by adding absorber on one side, but this reduces the gain and causes the system temperature to increase by 150 K for an ambient temperature system. A sinuous structure can be created on a cone to give a front-to-back ratio of about 10 dB [13]. The disadvantage of this method is that the phase center moves with frequency and hence, when used with a parabolic reflector, the feed must be moved mechanically to achieve optimum performance at each frequency. The front-to-back ratio depends on the taper angle and requires a steep taper to achieve a good ratio which, in turn, makes the feed very large. A planar antenna above a ground plane can remove all of the above problems but limits the bandwidth to less than an octave.

Our approach uses an inverted cone above a ground plane to obtain an unidirectional antenna. For a given frequency, a pair of $\lambda/2$ resonators in the opposite arms along with their images produce a beam at boresight. The cone angle is selected such that each pair of active resonators is a quarter wavelength above the ground plane. As a result, their images are also quarter wavelength below the ground plane and the overall phasing produces a beam at boresight. The phase center stays confined around the ground plane as a function of frequency due to the symmetry of the structure. Since the structure is defined by angles and expansion parameter τ, it follows the concept of frequency independence and the beam pattern should be invariant over the frequency range.

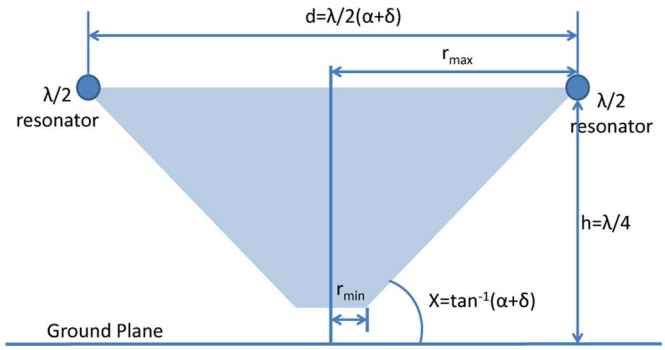

Fig. 2. Geometry showing parameters used in Table I.

TABLE I
PARAMETERS USED FOR THE THREE CASES TO STUDY THE EFFECT OF INTERLEAVING ON INPUT IMPEDANCE

name	0.5λ	0.6λ	0.75λ
$\alpha+\delta$ [rad]	1	0.83	0.66
cone angle X [degrees]	45	39.8	33.6
r_{max} [mm]	27	32	41
r_{min} [mm]	5	5	5
return loss [dB]	4	7	10

III. PARAMETER STUDY TO IMPROVE INPUT IMPEDANCE

A self-complementary conical sinuous antenna in free space offers frequency independent input impedance. Presence of a ground plane near such a self-complementary structure destroys the self-complementary nature of the composite structure causing the impedance circle to grow in diameter on a Smith Chart as can be seen in our early investigations [7], [8]. A change in terminal impedance Z_s as a function of frequency causes $|Z_s - Z_{\rm opt}|^2$ to change resulting in a ripple in the system noise, where $Z_{\rm opt}$ is the optimum impedance for lowest noise figure.

In order to address this problem, we conducted a parameter study where the self complementary condition of the antenna is relaxed. By reducing $\alpha+\delta$, angular width of the resonator can be reduced which in turn decreases the interleaving between the adjacent arms. The effect of interleaving between adjacent arms on the input impedance is studied using the 3D electromagnetic simulator CST Microwave studio. Three cases with successively less interleaving are presented here. The resonator length is equal to $\lambda/2$, the height above ground plane is $\lambda/4$ and $\alpha = 2\delta$ in all three cases. As the interleaving between adjacent arms is reduced, the distance between the opposite arms increases and the cone angle from ground plane decreases as shown in Fig. 2. We refer to the three cases according to the distance between opposite arms as 0.5λ, 0.6λ and 0.75λ. Table I summarizes the important parameters used in the three cases and the resulting return loss.

Fig. 3 shows the resulting structures in the three cases. Only five resonators are used in each structure to reduce simulation time. $r_{\max}$ is adjusted such that the lower cutoff frequency, given by (4) for all the structures is the same and is equal to 2.7 GHz. All were simulated from DC to 8 GHz. The input impedance for the three cases is shown in Fig. 4 on a 260 Ω Smith Chart. The impedance starts as a open circuit at DC and spirals in up to the lower cutoff frequency of 2.7 GHz. It then rotates around in a circle up to the upper cutoff frequency. The diameter of the impedance circle shrinks and the center of the circle becomes complex (includes capacitive reactance) as the interleaving is reduced. A significant improvement in input return loss can be seen for the 0.75λ case as shown in Fig. 6. If the

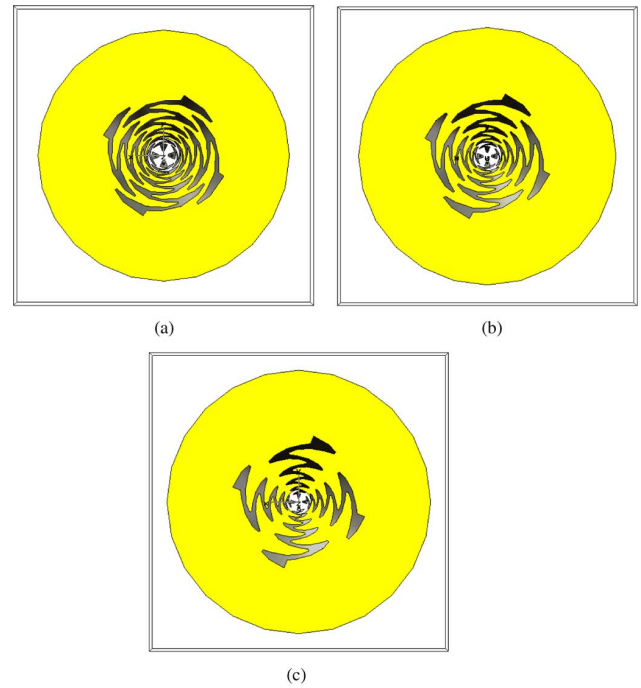

Fig. 3. Three sinuous structures with successively less interleaving are used for parameter study. The distance between opposite arms increases and the cone angle from ground plane decreases where the scaling is shown in Fig. 2 and the actual values can be read from Table I. (a) 0.5λ case, (b) 0.6λ case, (c) 0.75λ case.

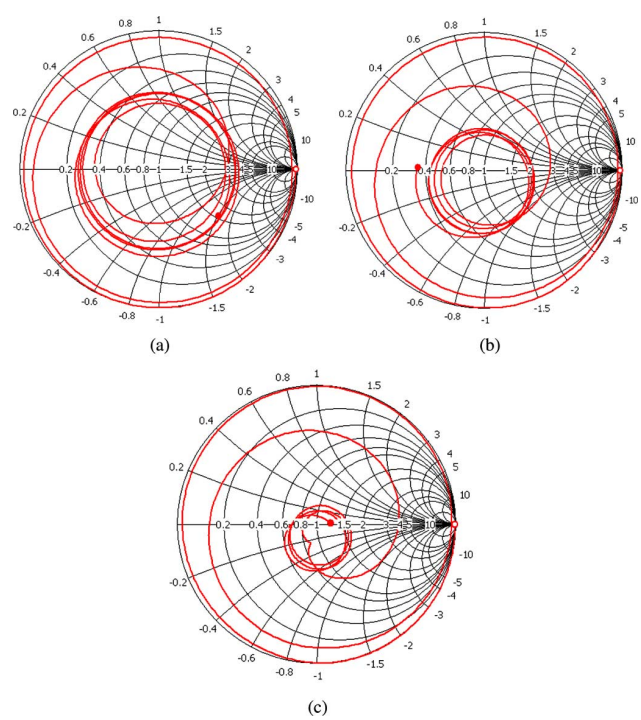

Fig. 4. Simulated sinuous antenna input impedance on a 260 Ω Smith Chart over DC-8 GHz frequency range. (a) 0.5λ case, (b) 0.6λ case, (c) 0.75λ case.

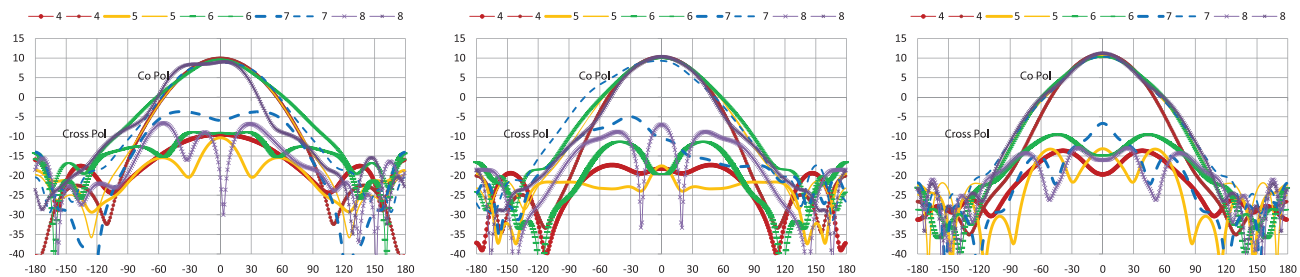

(a) 0.5λ case (b) 0.6λ case (c) 0.75λ case

Fig. 5. Simulated Co- and cross-polarized far field patterns in dB from 4 to 8 GHz as a function θ.

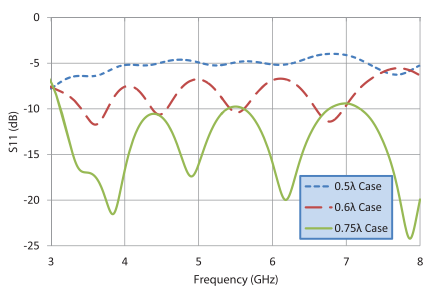

Fig. 6. Simulated magnitude of the sinuous antenna input reflection coefficient over DC—8 GHz frequency range for the three cases.

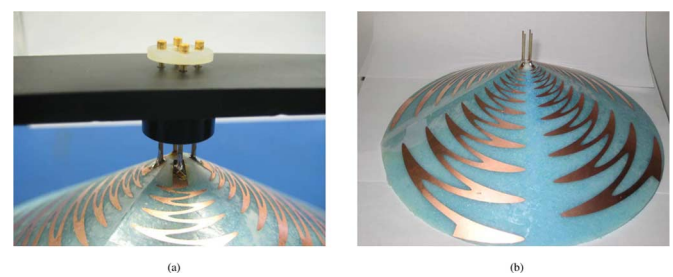

Fig. 7. Sinuous antenna assembly. (a) Jig used for assembly and feed point details, (b) sinuous feed without the ground plane and support.

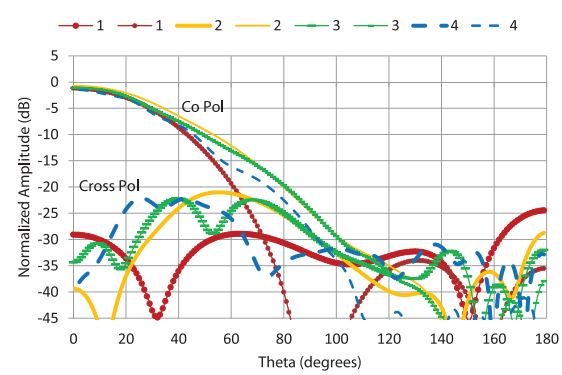

Fig. 8. Simulated Co- and Cross Polarization far field patterns in the 45° plane from 1 to 4 GHz.

interleaving is reduced further by decreasing the angular width of the arm, the operational mode changes to become a dipole like structure as the limiting case. There exists an optimal angular width for which the input return loss is maximum. Our simulations indicate this value is achieved close to the 0.75λ case. Fig. 5 shows the co- and cross-polarized far field patterns over the 4 to 8 GHz range.

IV. Antenna Performance

A. Antenna Assembly

Based on the results of the parameter study, the 0.75λ configuration is used to design an experimental 1 to 3 GHz feed. The antenna is fed using a pair of twin lines composed of two copper wires 1 mm diameter each separated by 7 mm in air. The simulated impedance of the twin line is 266 Ω. To maintain the distance between the copper wires a jig made from Delrin was used during assembly to hold and align the pins. Details of the feed point and jig are shown in Fig. 7(a). The completed sinuous antenna without the ground plane is shown in Fig. 7(b). A 64 cm × 44 cm rectangular ground plane is used for simulations and measurements to keep the overall size small during characterization.

B. Simulations

The sinuous feed is modeled using CST Microwave Studio. Based on the measurements of the previous versions of the feed, the simulation results are in good agreement with the measurements. The feed has additional short resonators at higher end to provide a smooth transition from the feed-point. The simulated results for the feed shown in Fig. 7(b) are presented from 1 to 4 GHz here. Fig. 8 shows the co- and cross-polarization far field patterns over 1 to 4 GHz in the 45° plane. The effect of truncated ground plane can be recognized in the narrowing of the beam at the lowest frequency at the expense of increased side lobe response. This is an edge effect and can be removed easily by expanding the ground plane. The E field orientation can be determined by taking the $\tan^{-1}$ of the ratio of the co- and cross-polarization amplitudes. The polarization wobbles $\pm 4°$ as a function of frequency. Fig. 9 shows the input reflection coefficient computed with a 260 Ω characteristic impedance and Fig. 10 shows the on axis directivity of the feed as a function of frequency. A return loss better than 9 dB and directivity constant within 1 dB can be seen over the whole bandwidth.

This feed will be used to illuminate a paraboloidal reflector. To characterize the feed, various sub-efficiencies are calculated as a function of parabola flare angle (or f/D ratio). Power radiated in higher order azimuthal variations cannot contribute to the gain of a symmetrical reflector antenna and hence is treated

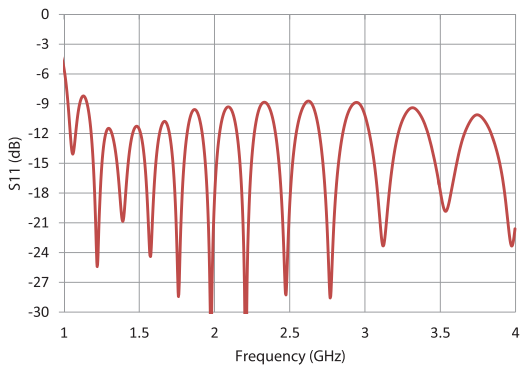

Fig. 9. Simulated input reflection coefficient for a 260 Ω characteristic impedance from 1 to 4 GHz.

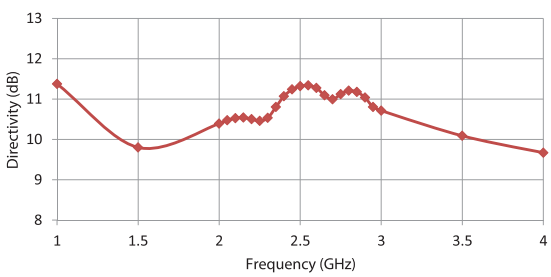

Fig. 10. Simulated on axis directivity as a function of frequency from 1 to 4 GHz.

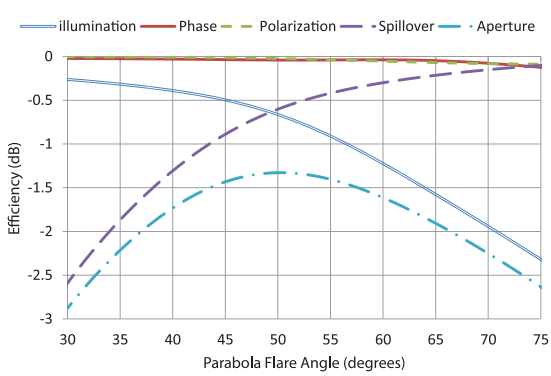

Fig. 11. Simulated sub-efficiencies using BOR1 components as a function of parabola flare angle.

as a BOR_1 efficiency as described in [15]. The BOR_1 components are extracted from the pattern and used to calculate the feed sub-efficiencies [16]. Since the patterns are frequency independent, the sub-efficiencies will be very close from one frequency to the next and hence not shown as a function of frequency here.

The strength in BOR_1 components is expressed as an efficiency and $\epsilon_{BOR_1} = 0.9414$. Fig. 11 shows the spill-over, illumination (or taper), polarization and phase efficiency along with the aperture efficiency which is given by the product of all sub efficiencies. The phase center is calculated as described in [17]. The phase center stays confined to $\pm 0.15\lambda$ around the ground plane.

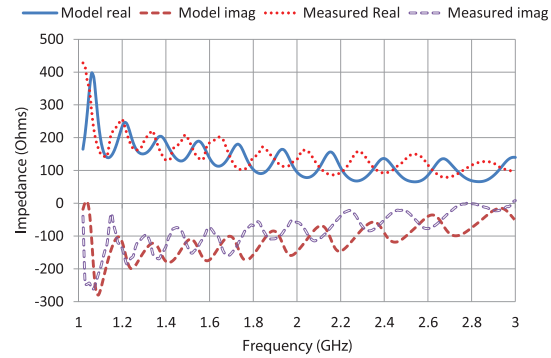

Fig. 12. Real and imaginary parts of the antenna input impedance. Comparison of measured and modeled values from 1 to 4 GHz.

C. Measurements

For the measurement purpose, the antenna was fed using a coaxial fixture in a single ended mode. The VNA was calibrated at the coaxial ports using a standard calibration kit to measure two port S parameters. The coaxial fixture was then de-embedded to get the two port S parameters at the antenna feed terminals and the differential-mode reflection coefficient was obtained according to [18]. The real and imaginary parts of the measured and modeled input impedances between the arms are compared from 1 to 3 GHz in Fig. 12. The general trend of the simulation and measurement is in agreement. There is a phase shift between measured and modeled data which increases as the frequency increases. We think the disagreement between measurement and simulation is a result of permittivity values of the dielectric materials that differ somewhat from the generic values in the simulation.

V. Amplifier Design and Assembly

Integration of the LNA and the feed is vital to the overall performance of the receiving system. Any connectors between the feed and LNA act as lengths of transmission lines with an impedance other than the antenna impedance. This produces a rotation and transformation of the antenna impedance on the Smith Chart that is frequency dependent. The modified input impedance is presented to the LNA which differs from the impedance for which the LNA is designed resulting in an overall higher system noise temperature.

Fig. 13 shows the block diagram of the feed-LNA integration. This arrangement avoids any crossover before the LNAs. A single ended LNA was attached to each of the four arms of the feed. The outputs of the LNAs in opposing arms were combined using a commercial 180° hybrid [19] at Δ ports and the Σ ports were terminated using 50 Ω resistors. Although the input to this arrangement is differential, it is not a true differential amplifier. We refer to this arrangement as pseudo differential amplifier since a low impedance, real ground is introduced at the input of the single ended amplifiers in contrast with a high impedance virtual ground in the true differential amplifier. This configuration helps to reduce undesired effects of the even mode by providing a low impedance path at the Σ port. The real ground also

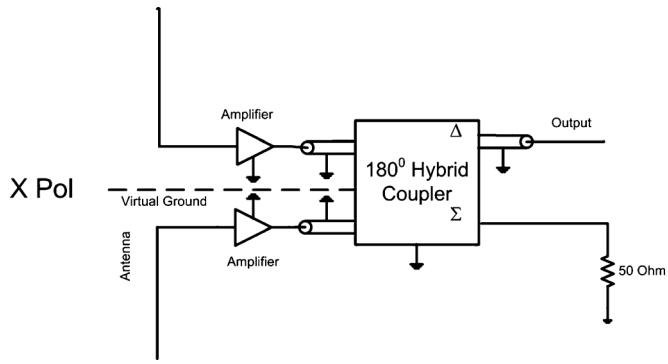

Fig. 13. Integrated feed-LNA configuration for the X polarization. Similar configuration is used for the Y polarization.

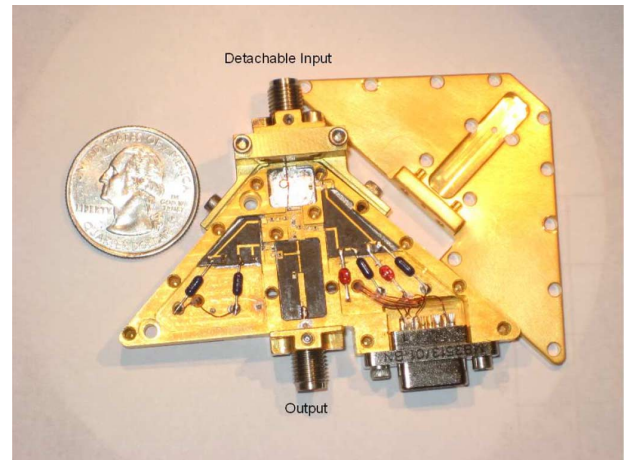

Fig. 15. Photograph of the LNA.

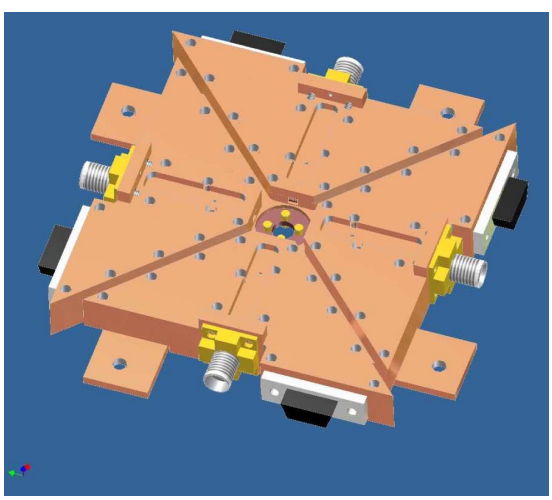

Fig. 14. Inventor drawing showing chassis holder used for LNA feed integration.

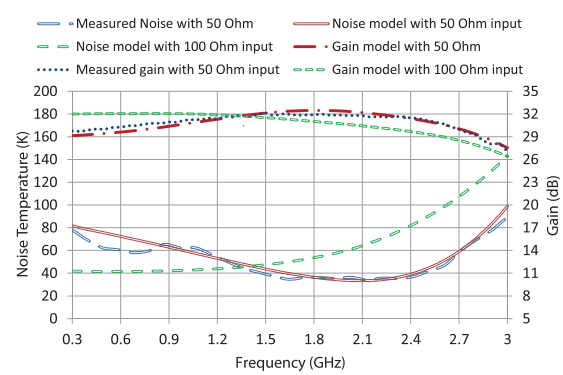

Fig. 16. Measured and modeled noise and gain in 50 Ω system. Modeled noise and gain with 100 Ω input impedance.

provides better isolation. The two pseudo differential amplifier outputs provide two linear polarizations.

A chassis holder was designed to mount four LNAs radially outwards as shown in the Fig. 14. A circular G10 board with four holes and a hole in the center is mounted at the center of the holder. Four receptor are fitted in the four holes which can accept the twin lines. The receptors have spring contacts which assures easy assembly and disassembly of the feed and LNA. This type of unconventional assembly procedure ensures that the antenna input impedance is carried through to the transistors.

A low noise amplifier was developed using Eudyna FHX45X GaAs super high electron mobility transistors (HEMT) optimized for an input impedance of 100 Ω. Agilent's Advanced Design System (ADS) was used for the design and modeling. Fig. 15 is a photograph of the amplifier. The LNA was designed for the higher antenna input impedance but the measuring system is 50 Ω. A detachable input was designed for the characterization of the LNA in the 50 Ω environment. Fig. 16 shows the modeled and measured noise temperature as well as gain as a function of frequency.

VI. Receiver Noise

The noise produced by the feed-LNA combination was measured using the Y-factor method with the sky as the cold load and ambient temperature absorber as the hot load. In the Y-factor method, the output powers $P_{\rm cold}$ and $P_{\rm hot}$ are measured with the antenna exposed to the cold load and the hot load, respectively. The ratio of the two is called the Y-factor. Based on the temperatures of the hot and cold loads, the receiver noise can be calculated as [20]

$$T_R = \frac{T_{\rm hot} - YT_{\rm cold}}{Y-1} \tag{5}$$

The possible sources of error in this measurement method include

1) the uncertainty in the $T_{\rm cold}$ and $T_{\rm hot}$ temperatures;
2) the presence of radio frequency interference (RFI);
3) the area covered by the absorber, which determines what part of the main beam is looking at the $T_{\rm hot}$ (A small area will in turn lower the effective $T_{\rm hot}$ and need to be corrected using the beam pattern of the antenna);
4) the size of the absorber, which should be large enough to offer sufficient absorption at the lowest frequency used in the measurement;

5) the distance between feed and the absorber, which should be a sufficient distance to make sure that the antenna impedance is not influenced, which can easily be verified;
6) the contribution from the mountains on the horizon and ground, which may lead to a higher $P_{\rm cold}$.

A. Measurement Procedure

In order to reduce the effect of RFI, the measurement was performed at the NRAO, Green Bank site which is located in the National Radio Quiet Zone (NRQZ). The measurement was carried out after sunset inside an empty parking lot away from any large structures. Agilent's N8973A noise figure analyzer (NFA) was used in power measurement mode for the test. A preamplifier was used before the NFA to increase the gain and reduce the effect of instrument noise. Attenuators were used between the stages to reduce mismatch ripple. A carefully measured attenuator was added and removed before the preamp and the difference in power was compared to the attenuation to ensure linear operation.

The NFA offers RF and IF attenuation which can be set automatically or manually. For a given frequency, with the hot load over the feed, $P_{\rm hot}$ was recorded with the RF and IF attenuation on "auto". The RF and IF attenuation was then held constant for rest of the measurement for that frequency. With the hot load moved sufficiently away from the antenna, $P_{\rm cold}$ was recorded. The procedure needs to be repeated for each frequency point. The data were collected every 25 MHz from 1.3 to 2.8 GHz which is a time consuming process but necessary to ensure the ripple in noise was properly sampled. Noise was sampled at every 100 MHz near the edges of the band.

B. Corrections to $T_{\rm hot}$ and $T_{\rm cold}$

The antenna temperature T_A due to a source at temperature $T_s(\theta,\phi)$ is given by [21]

$$T_A = \frac{A_e}{\lambda^2}\int\int T_s(\theta,\phi)P_n(\theta,\phi)\,d\Omega \tag{6}$$

where A_e is the effective aperture of the antenna, λ is the wavelength, $P_n(\theta,\phi)$ is the normalized antenna power pattern and $d\Omega = \sin\theta d\theta d\phi$ in the spherical co-ordinate system. During the hot and cold measurements, the antenna main beam was pointed at the hot source and the cold source but the output power received contributions from the side-lobes and the back-lobe which are not necessarily seeing the same source. Fig. 17 shows the approximate contributions from the side and back lobes for the hot case. This leads to an equivalent temperature $T_{\rm hoteqv}$ that is lower than $T_{\rm hot}$. Similarly in the cold case, contributions from ground leads to an equivalent temperature $T_{\rm coldeqv}$ that is greater than $T_{\rm cold}$. $T_{\rm hoteqv}$ and $T_{\rm coldeqv}$ should be used during the Y-factor measurement.

The equivalent hot and cold temperatures can be estimated using the antenna pattern in (6). Assuming concentric rings of source temperature removes the effect of ϕ in the integral. After canceling the common terms, for the hot case

$$T_{\rm hoteqv}\int_0^{180} P_n(\theta)\sin\theta d\theta = T_{\rm hot}\int_0^{\theta_1} P_n(\theta)\sin\theta d\theta$$

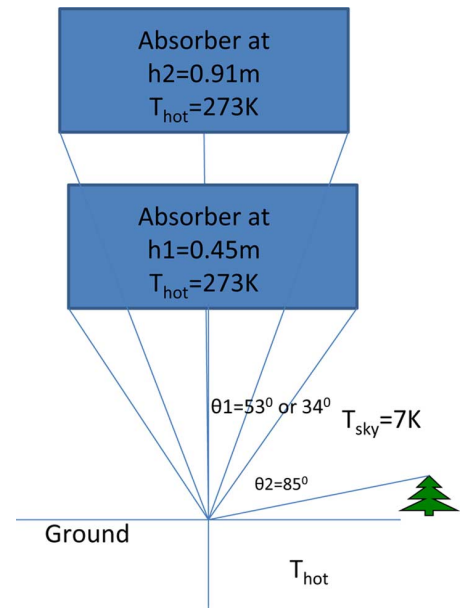

Fig. 17. Geometry showing absorbers at different heights and sidelobe contributions.

$$+T_{\rm cold}\int_{\theta_1}^{\theta_2} P_n(\theta)\sin\theta d\theta + T_{\rm hot}\int_{\theta_2}^{180} P_n(\theta)\sin\theta d\theta \tag{7}$$

where the integrals can be solved numerically using the pattern data and the equation can be solved to obtain $T_{\rm hoteqv}$. Similarly, $T_{\rm coldeqv}$ can be found for the cold case.

We calculated the equivalent temperatures using Matlab for the E-plane, H-plane and used the average value in the T_R calculation using $T_{\rm hot} = 273$ K and modeling sky as $T_{\rm cold} = 7$ K [21] from 1 to 3 GHz. As a cross check for using the equivalent temperatures in the receiver noise calculation a second measurement was performed with the absorber at a different height, $h2 = 0.91$ m as shown in Fig. 17. With the same absorber at a larger distance from the antenna, the main beam also sees the cold sky resulting in different equivalent temperatures. Table II summarizes the calculated equivalent temperatures for the two cases for both E-plane and H-plane. Fig. 18 shows the measured and modeled receiver noise over 1 to 3 GHz range. The measurement includes the second stage contribution which is expected to be 5–10 K across the band. The model was obtained by applying the measured antenna input impedance to the LNA model in ADS assuming a 0.3 dB of loss in the antenna as suggested by the CST simulation of the antenna. A good agreement between modeled and measured results can be seen. The sharp spikes in the measured data can be attributed to the strong RFI present at those frequencies confirmed using a spectrum analyzer.

VII. Using the Feed on a Radio Telescope

The overall system performance of a radio telescope can be expressed as a $A/T_{\rm sys}$ ratio, where A is the effective area of the parabolic dish illuminated by a feed and $T_{\rm sys}$ is the system noise temperature [22]. The effective area for a paraboloid with physical aperture A_p and total efficiency $\epsilon_{\rm tot}$ is given by $A = \epsilon_{\rm tot}A_p$ where $\epsilon_{\rm tot}$ is a product of various sub-efficiencies.

$T_{\rm sys}$ can be divided into three parts as

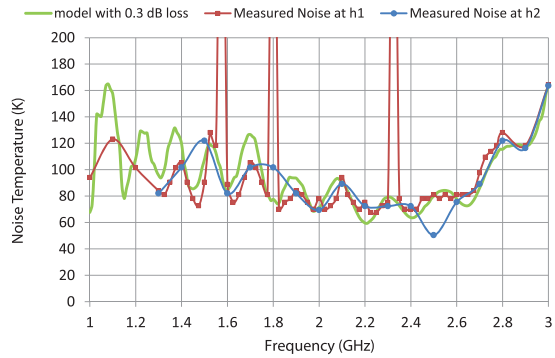

Fig. 18. Measured receiver noise for two cases in Table II and modeled receiver noise with 0.3 dB loss over 1–3 GHz frequency range.

TABLE II
EQUIVALENT TEMPERATURES FOR LONG AND SHORT ABSORBER CASES

	Absorber at $h1 = 0.45m$		Absorber at $h2 = 0.91m$	
	T_{hoteqv}(K)	$T_{coldeqv}$(K)	T_{hoteqv}(K)	$T_{coldeqv}$(K)
E-plane	241	11	164	11
H-plane	257	13	178	13
Average	249	12	171	12

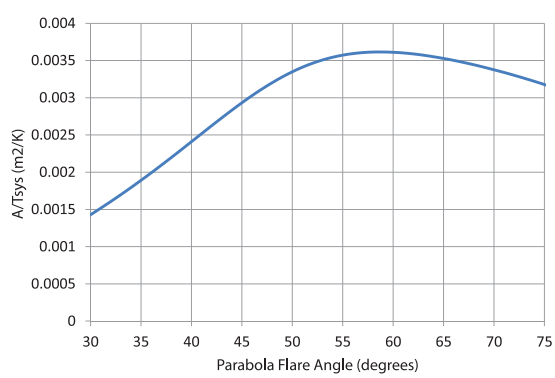

Fig. 19. Computed $A/T_{\rm sys}$ as a function of parabola flare angle.

$$T_{\rm sys} = T_R + T_{\rm spillover} + T_{\rm antenna} \tag{8}$$

where T_R is the measured noise as shown in Fig. 18, $T_{\rm spillover}$ is the temperature due to the part of the feed pattern that misses the parabola and is given by

$$T_{\rm spillover} = T_{\rm amb} p_g \tag{9}$$

where p_g is the fraction of the feed solid angle that illuminates the ground at temp $T_{\rm amb} = 290$ K. $T_{\rm antenna}$ is the antenna temperature given by

$$T_{\rm antenna} = T_{\rm sky}(1 - p_g) \tag{10}$$

where $T_{\rm sky} = 7$K is the sky temperature.

Considering the worst case axial displacement of the feed of 0.15 λ from the reflector focal point, a focal efficiency of 0.9 is obtained according to [15]. Based on these values, we have calculated $A/T_{\rm sys}$ as a function of parabola flare angle as shown in Fig. 19 for a 1 m diameter parabolic dish. This curve can be used to calculate the $A/T_{\rm sys}$ for any center fed parabola by multiplying it with the square of the diameter of the dish.

TABLE III
WORST CASE EFFICIENCIES FOR THE SINUOUS FEED FOR A PARABOLA FLARE ANGLE OF 60°

Sub-efficiency	Value	Value (dB)
BOR_1	0.94	-0.27
Spillover (ϵ_{sp})	0.93	-0.32
Illumination (ϵ_{ill})	0.75	-1.25
Polarization (ϵ_{pol})	0.99	-0.04
Phase (ϵ_{ϕ})	0.99	-0.04
Defocussing Loss (ϵ_{foc})	0.90	-0.46
Total Efficiency (ϵ_{tot})	0.58	-2.38

For example, the 43 m center fed radio telescope located in Green Bank, WV has a f/D of 0.43 or a parabola flare angle of 60.3°. Table III summarizes various sub-efficiencies for this angle. $T_R = 100$ K, $T_{\rm spillover} = 20.6$ K and $T_{\rm antenna} = 6.5$ K resulting in $T_{\rm sys} = 127.1$ K is used for this calculation. Using Fig. 19, we find $A/T_{\rm sys} = 43^2(0.0036) = 6.7$ m^2/K.

VIII. PROSPECTS

The basic operation of the conical sinuous feed over a ground plane was verified by characterizing pattern, input impedance and noise over 1 to 3 GHz frequency range using a physically small laboratory version of the sinuous antenna. Based on the experience gained from this work, it is possible to make improvements in terms of sensitivity and bandwidth to make it ideal for next generation of radio telescopes. The lowest frequency of operation is determined by the outer radius according to (4). We plan to develop a decade bandwidth feed by adding seven additional resonators using the current expansion parameter $\tau = 1.2536$. The antenna radius will increases from 113 mm to 550 mm while the height will increase from 75 mm to 363 mm enabling operation over 0.3 to 3 GHz frequency range.

The presence of a capacitive reactance, which is a result of departure from the self complementary structure diverges the input impedance when a length of line is added between the feed and LNA. The length of the line can be reduced to a minimum value by connecting LNAs right at the feed point. We plan to achieve this by thinning the ground plane in the center near the feed point. Reduction in line length not only provides better matching but will also reduce the loss at the feed point resulting in lower system noise. A state of the art transistor with a smaller $T_{\rm min}$ will directly translate into a reduced system noise temperature. With improvements in matching, antenna losses and using better transistors we envision an improved sensitivity for the decade bandwidth antenna.

The current system noise shows a ripple in the measured data which arises as a result of mismatch between the feed and the LNA. Although we have not done any stability measurements, we do not see any obvious sources that should cause the impedances to vary over time. It will be possible to calibrate the slope in the system noise using astronomical observations. The feed is very lightweight and mechanically stable, hence we don't anticipate deformation or effects such as sagging as the telescope points. The feed gets a natural insulation since it is encompassed inside a foam, which reduces the effect of temperature variations, if any, on the impedance.

Since the measurements are non standard, it takes a long time to make modifications based on the measurement results and the overall development process becomes slow. One of the big challenges in wideband feed development for future radio telescopes is to develop more efficient and faster ways to characterize the system.

IX. Conclusion

We have developed a sinuous-type wideband, dual linear polarized, fixed phase center, low loss feed with an integrated LNA. For the ease of integration and initial testing the feed size was kept small which limits the low frequency operation to about 1 GHz. The feed works from 1 to 3 GHz but we plan to increase the bandwidth to 10:1 in near future. Input return loss better than 9 dB is achieved over the whole bandwidth. The maximum aperture efficiency is around 0.7 and can be achieved over range of parabola flare angles between 45° to 55°.

A room temperature, low noise amplifier was developed using Eudyna FHX45X HEMTs optimized for the high antenna input impedance over 0.3 to 3 GHz frequency range. A system noise temperature in the range 70 K to 100 K is achieved over most of the band. The possible sources of error in the system noise measurement and precautions taken to mitigate them are listed.

To improve the sensitivity of the system further, a cryogenic version of this feed-LNA unit is under development.

References

[1] G. Engargiola, "Non-planar log-periodic antenna feed for integration with cryogenic microwave amplifier," in *Proc. IEEE Antennas and Propagation Society Int. Symp.*, 2002, vol. 4.

[2] R. Bradley, C. Parashare, S. M. White, and T. S. Bastian, "Instrument development for the green bank solar radio burst spectrometer (GB/SRBS)," in *ASP Conf. Series*, 2005, vol. 345.

[3] R. Olsson, P.-S. Kildal, and S. Weinreb, "The Eleven antenna: A compact low-profile decade bandwidth dual polarized feed for reflector antennas," *IEEE Trans. Antennas Propag.*, vol. 54, no. 2, pt. 1, pp. 368–375, Feb. 2006.

[4] J. Yang, X. Chen, N. Wadefalk, and P.-S. Kildal, "Design and realization of a linearly polarized eleven feed for 1–10 GHz," *IEEE Antennas Wireless Propag. Lett. (AWPL)*, vol. 8, pp. 64–68, 2009.

[5] ETS Lindgren, "Open boundary quad-ridged horn," 3164-06 Datasheet. [Online]. Available: http://www.ets-lindgren.com/pdf/3164-05.pdf

[6] G. Cortes-Medellin, "Input impedance characterization of the QSC ultra wide band feed," in *Proc. IEEE Antennas and Propagation Society Int. Symp.*, Jul. 5–11, 2008, pp. 1–4.

[7] R. S. Gawande and R. F. Bradley, "The inverted conical sinuous antenna over a ground plane," presented at the CNC/USNC—North American Radio Science Meeting (URSI), Ottawa, Canada, Jul. 2007 [Online]. Available: www.astro.caltech.edu/USNC-URSI-J

[8] R. S. Gawande and R. F. Bradley, "Characterization of the inverted, conical, sinuous antenna—amplifier integrated unit," presented at the XXIX General Assembly of the Int. Union of Radio Science (URSI), Chicago, Aug. 2008.

[9] Y. Mushiake, "Self-complementary antennas," *IEEE Antennas Propag. Mag.*, vol. 34, pp. 23–29, 2002.

[10] X. Dardenne and C. Craeye, "Simulation of the effects of a ground plane on the radiation characteristics of self-complementary arrays," in *Proc. Antennas and Propagation Society Int. Symp.*, 2003, vol. 1, pp. 383–386.

[11] R. S. Gawande and R. F. Bradley, "G/T sensitivity comparison of different topologies using ultra wide band, active, conical sinuous antenna," presented at the IEEE AP-S URSI, Jun. 2009.

[12] R. H. DuHamel, "Dual Polarized Sinuous Antennas," U.S. Patent 4 658 262, Apr. 14, 1987.

[13] R. C. Johnson, *Antenna Engineering Handbook*, 3rd ed. New York: McGraw-Hill , 1993.

[14] J. A. Huffman and T. Cencich, "Modal impedances of planar, non-complementary, n fold symmetric antenna structures," *IEEE Antennas Propag. Mag.*, vol. 47, no. 1, Feb. 2005.

[15] P.-S. Kildal, *Foundations of Antennas—A Unified Approach*. Lund, Sweden: Studentlitterature, 2000.

[16] P.-S. Kildal, "Factorization of the feed efficiency of paraboloids and Cassegrain antennas," *IEEE Trans. Antennas Propag.*, vol. Ap-33, no. 8, pp. 903–908, Aug. 1985.

[17] P.-S. Kildal, "Combined E- and H-plane phase-centers of antenna feeds," *IEEE Trans. Antennas Propag.*, vol. AP-31, no. 1, pp. 199–202, Jan. 1983.

[18] W. Fan, A. Lu, L. L. Wai, and B. K. Lok, "Mixed-mode S-parameter characterization of differential structures," in *Proc. Electronics Packaging Technology, 2003 5th Conf. (EPTC 2003)*, Dec. 10–12, 2003, pp. 533–537.

[19] ET Industries, "180 degree hybrid coupler-stripline design datasheet," J-058-180 Datasheet [Online]. Available: http://www.etiworld.com

[20] Agilent Technologies, "Noise figure measurement accuracy—The Y-factor method," Application Note 57-2.

[21] J. D. Kraus, *Radio Astronomy*, 2nd ed. Columbus, OH: Cygnus-Quasar Books, 1986.

[22] *IEEE Standard Definitions of Terms for Antennas*, IEEE Std 145-1993, 1993.

Rohit S. Gawande (S'08) received the B.E. degree from the Government College of Engineering, Pune, India, in 2002, and the M.Sc. degree in radio astronomy and space science from Chalmers University of Technology, Gothenburg, Sweden, and the M.S. degree in electrical engineering from California Institute of Technology, Pasadena. He is currently working toward the Ph.D. degree at the University of Virginia, Charlottesville, with his dissertation work at the National Radio Astronomy Observatory, Charlottesville.

His research interests include radio astronomy instrumentation, wideband antennas and room temperature and cryogenic low noise amplifiers.

Richard F. Bradley (S'81–M'84) received the B.S.E.E and M.S.E.E degrees from Carnegie-Mellon University, in 1982 and 1983, respectively, and the Ph.D. degree in E.E. from the University of Virginia, Charlottesville, in 1992.

In 1992, he joined the National Radio Astronomy Observatory, Charlottesville, VA, where he is currently a Staff Scientist and Research Engineer. He is also a Research Professor in the Department of Astronomy and holds an adjunct faculty position in the Department of Electrical and Computer Engineering at the University of Virginia. His research interests include radio astronomy, scientific instrumentation, low noise electronics, electromagnetic fields, and signal processing. He has over 75 research publications and holds one patent.

Dr. Bradley is the Chair of Commission J, U.S. National Committee for the International Union of Radio Science (URSI) and is an Associate Editor of the *Journal Radio Science*.